Comparison of C-V measurement methods for RF-MEMS capacitive switches

Jiahui Wang, Cora Salm, and Jurriaan Schmitz

MESA+ Institute for Nanotechnology, University of Twente

Enschede, the Netherlands

Fax: +31 534891034. Email: j.wang-1@utwente.nl

***Abstract*—The applicability of several capacitance-voltage measurement methods is investigated for the on-wafer characterization of RF-MEMS capacitive switches. These devices combine few-picofarad capacitance with a high quality factor. The standard quasistatic and high-frequency measurements are employed, as well as the recently introduced very-low-frequency method. S_{11} is measured by a network analyzer to calculate the capacitance of the device from radio-frequency measurements. Significant differences are found around the pull-in and pull-out voltages.**

Keywords—RF-MEMS switch; capacitance; parasitics; measurement

I. INTRODUCTION

RF-MEMS capacitive switches and varactors have penetrated the high-volume handset market in 2011 [1]. These new devices combine a high tuning ratio with a good quality factor (see e.g. [2]), making them an attractive choice for tunable impedance matching at the antenna. For process development and process control, electrical testing at wafer level of these components is essential, but is confronted with three major issues: the device is very sensitive to the ambient before packaging, it has a relatively low total capacitance of only a few picofarad, and its mechanical behavior has a very long time scale compared to other microelectronic components, in the millisecond range [3].

In this paper we will present a measurement approach which effectively tackles the ambient issue with a standard wafer-level probe station, and show and compare capacitance-voltage (*C-V*) measurements on RF-MEMS capacitive switches using the quasistatic, very-low-frequency, high-frequency and radio-frequency *C-V* measurement techniques.

II. EXPERIMENTAL

The RF-MEMS capacitive switches were fabricated on a Si substrate. Fig. 1 shows the top view of the RF-MEMS capacitive switch designed for ground-signal-ground (GSG) probing. The large perforated square (300 x 300 μm^2) is the moving electrode, connected to ground; the underlying firm electrode is connected to the signal (S) pad. The movable top electrode is connected to four anchors by the curved springs. All metallization is aluminum. The devices (and open/short de-embedding structures) are contacted with two micromanipulators, with the exception of the RF-CV measurement where a GSG probe was used.

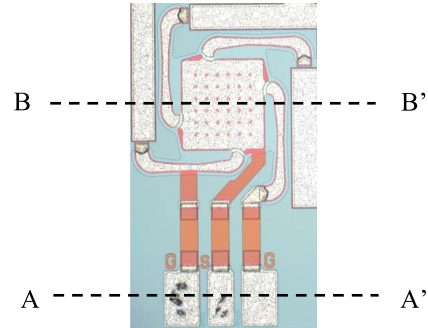

Fig. 1 Top view microscope image of the RF-MEMS capacitive switch under study. The A-A’ and B-B’ dashed lines indicate the cross-sections of figures 2 and 3.

A Keithley 595 Quasistatic meter (QSCV) was used for the quasistatic *C-V* measurement. Both an HP 4284A LCR meter (LCR) and a Keithley SCS 4200 (K4200) were used for the high-frequency *C-V* measurement.

The very-low-frequency (VLF) measurements [4] were conducted using the Keithley SCS 4200 with two pre-amplifiers. In the set-up of the VLF measurement, starting values for capacitance and resistance should be given. Only with well-chosen values (from previous measurements or calculated estimates) we obtain good convergence towards the expected capacitance.

A ZVB20 network analyzer [5] was used for 1-port radio-frequency *C-V* (RF-CV) measurement. Open/short/load calibration is carried out on a standard calibration pattern. The test structure parasitics are consecutively eliminated by de-embedding (as described later). The device impedance is calculated from S_{11} by the following equations [6]:

$$Z_m = 50\Omega \times \frac{1+S_{11}}{1-S_{11}}$$

$$Z_{\mathrm{DUT}} = \frac{Z_{\mathrm{o}} \times (Z_{\mathrm{mDUT}} - Z_{\mathrm{s}})}{Z_{\mathrm{o}} - Z_{\mathrm{mDUT}} + Z_{\mathrm{s}}} \qquad C_{DUT} = \frac{-1}{2\pi f \times \mathrm{Im}(Z_{\mathrm{DUT}})}$$

where Z_{DUT} is the impedance of the device under test; Z_{o} is open compensation; Z_{s} is the short compensation; Z_{mDUT} is the measured impedance of the device under test; Z_{m} is the measured impedance.

To remove any moisture, which is the main cause of stiction failure, a 10 minutes dry air flush at room temperature is employed followed by a 10 minutes heating step in dry air at

150 °C. All measurements were at room temperature with dry air flow. The measured capacitance kept stable when we repeated the *C-V* measurement. This indicates that no change of the device occurred during the measurement.

III. EXPERIMENTAL RESULTS

A. Device and system parasitics

A careful de-embedding is needed to get the accurate capacitance of the device under test (C_{DUT}), because the parasitic capacitance is of the same order as the DUT capacitance. The schematic cross sectional view of the bond pad area (A-A') is shown in Fig. 2 (a). Parasitic capacitance exists between the bond pads, through air and through the silicon substrate. Given that the outer pads are both grounded, the equivalent circuit in the bond pad area A-A' can be simplified as shown in Fig. 2 (b).

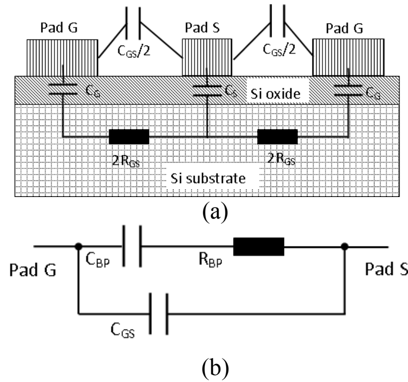

Fig. 2 (a) The schematic cross sectional view of the device from A-A' of Fig. 1, (b) the small-signal equivalent circuit of the parasitics.

The schematic cross sectional view of the device at B-B' is shown in Fig. 3 (a). Besides the device capacitance under study C_{DUT}, parasitic capacitance is found around the switchable electrode via the substrate. Given the symmetry, again the parasitic equivalent circuit can be simplified as the sub-circuit of C_{BE+} and R_{BE}, as shown in Fig. 3 (b).

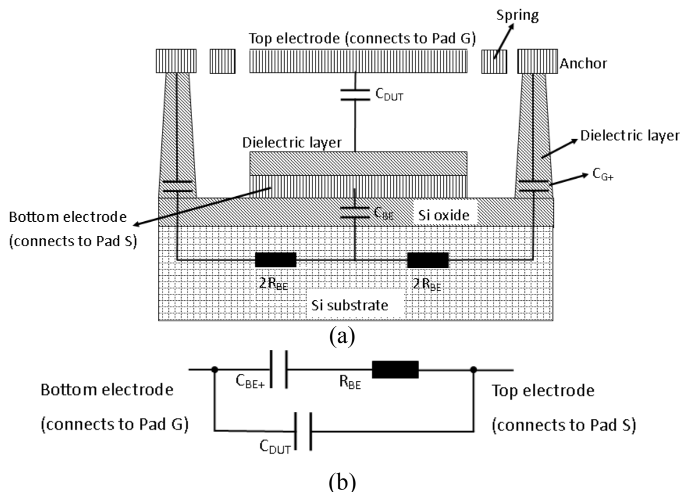

Fig. 3 (a) The schematic cross sectional view of the device from B-B' of Fig. 1, (b) the small-signal equivalent circuit of the parasitics.

Apart from the parasitics shown in Fig. 2 and Fig. 3, there are cable inductance (L_{SYS}), pad-to-probe resistance (R_{SYS}) and open capacitance (C_{SYS}) outside the test structure; and there are short inductance (L_s) and resistance (R_s) introduced by the connection lines between the pads and the device. A total equivalent circuit is shown in Fig. 4 by combining all parasitics.

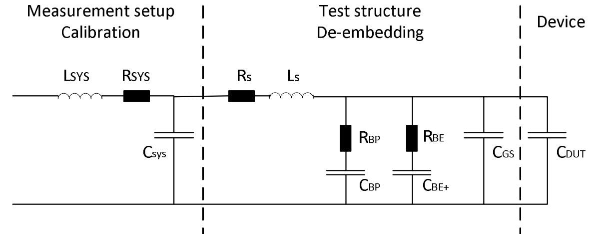

Fig. 4 The small-signal equivalent circuit of parasitics of the device and measurement system.

The device is larger at B-B' than at A-A'. As a consequence, the RC-times of the parasites $R_{BP}C_{BP}$ and $R_{BE}C_{BE+}$ are significantly different. In a device study across a large frequency range, this may lead to different open capacitance corrections for different regimes.

The open–correction is capacitive at our measurement frequency range from quasi-static to 1 GHz. Several reference structures were available on-wafer for open de-embedding, but no structure was designed such that an accurate open correction could be obtained for all measurements. Hence, one DUT was sacrificed to the purpose: the top electrode was mechanically removed from the device, and the damaged structure was then used as the open reference [7]. This approach does disconnect the two ground pads, so we divided the obtained open impedance by two when the devices were probed with two micromanipulators (for QSCV, VLF and high-frequency measurements). For radio-frequency measurements, the two ground pads are connected using the GSG probe, so the obtained "open" capacitance is correct.

The short compensation is only important in radio-frequency measurement. We found a significant difference between the device's parasitic inductance and that of the provided "short" reference structure on the wafer. By estimation of the induction-loop areas of the DUT and the "short" test structure, L_s as obtained from the short measurement could be corrected manually (multiplying L_s with the loop area ratio). With the corrected L_s value, the capacitance became frequency independent.

Exemplary capacitance-frequency curves of the device, obtained by the five measurement techniques, are shown in Fig. 5. In this figure, obtained capacitance values in the "up" and "down" state of the switch are shown from all five measurement approaches. As the quasistatic measurement does not associate with a measurement frequency, the QSCV values are indicated with dashed lines. High-frequency measurements (using LCR and K4200) below 10 kHz were inaccurate, as the device capacitance is too low. Hence these data are not shown here.

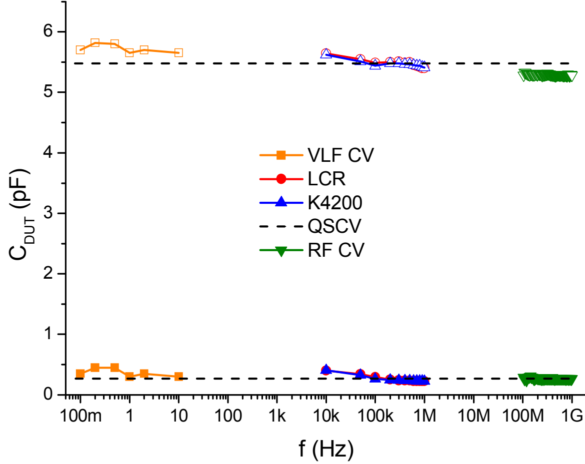

Fig. 5 The device capacitance as a function of frequency, as determined by the five measurement approaches. The capacitance is almost independent of frequency. The open-symbol measurements are obtained under DC bias of -15 V, while the solid symbols represent measurements at 0 V bias.

The obtained average value of C_{DUT} is 5.65 pF and 0.3 pF at down-state and up-state, respectively, almost independent of frequency. This indicates an accurate de-embedding. However, in the full *C-V* curve we did observe distinct differences. These are treated in the next subsection.

B. C-V Comparison measured by five approaches

Fig. 6 shows full *C-V* curves measured by these five approaches. Upon closer inspection, the *C-V* curves measured by different instruments exhibit some differences, in particular near the pull-in and pull-out voltages (V_{pi}, V_{po}). In Fig. 6, the voltage region between -15 V and -8 V shows distinctly different curves for HF and RF capacitance (gradually going down) on one hand, and QSCV and VLF capacitance (remaining constant, then going up) on the other hand.

This gradual capacitance decrease with reducing electric field in the downstate is commonly and consistently observed on RF MEMS capacitive switches. It is attributed to the flattening of the dielectric-metal interface or zipping effects [8-12].

However, in the QSCV and VLF measurements, the C_{DUT} at down-state does not decrease with the absolute value of DC bias voltage close to the pull-out voltage. Instead, C_{DUT} increases when the DC bias is close to V_{po}, so either the measured values are incorrect, or the commonly accepted contact model is at least incomplete.

It should be noted that the quasistatic measurement is error-prone upon the sudden switching of the device, where the assumption of quasistatic conditions does not hold. (At pull-out, an infinitesimal change in DC voltage leads to a large capacitance change.) This however does not explain any discrepancies seen several measurement points away from V_{po}.

The VLF and QSCV measurements typically have a slower voltage sweep than the high-frequency methods. We investigated whether the different measurement time scale is the cause for this effect, by artificially slowing down the high-frequency *C-V* sweeps. The measurement time does not influence the *C-V* curve in these high-frequency measurements even with 4 seconds hold time and 4 seconds wait time.

A more detailed comparison of the *C-V* curves near V_{po} is shown in Fig. 7. In RF, K4200 and LCR measurements, C_{DUT} decreases with an average rate of 0.025 pF/V between -20 V and -11 V. The decrease is somewhat faster between -11 V and V_{po} (see Figs. 7a–c). In the VLF measurements (Fig. 7d), C_{DUT} decreases with a slower rate of 0.02 pF/V from -20 V to -11 V (independent of the frequency). Between -11 V and V_{po}, C_{DUT} increases with DC bias voltage. The QSCV measurement is similar (Fig. 7e), be it somewhat obscured by the lower measurement accuracy.

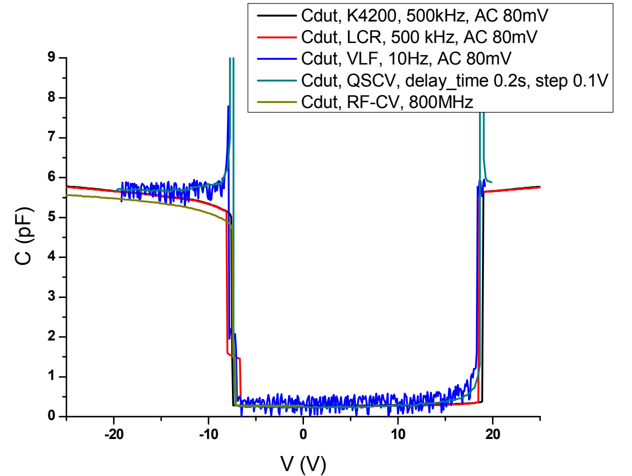

Fig. 6 Comparison of the *C-V* curves measured by five approaches.

This *C-V* behavior has been observed consistently on various devices under test. Further, no measurement-induced device changes have been observed on any of the measurement techniques or devices.

From our experiments reported above, we can rule out the measurement time and measurement-induced device changes as causes for the observed discrepancy between high-frequency and low-frequency measurements in the voltage range between -11 V and V_{po}. But otherwise, the origin if this discrepancy is still unclear.

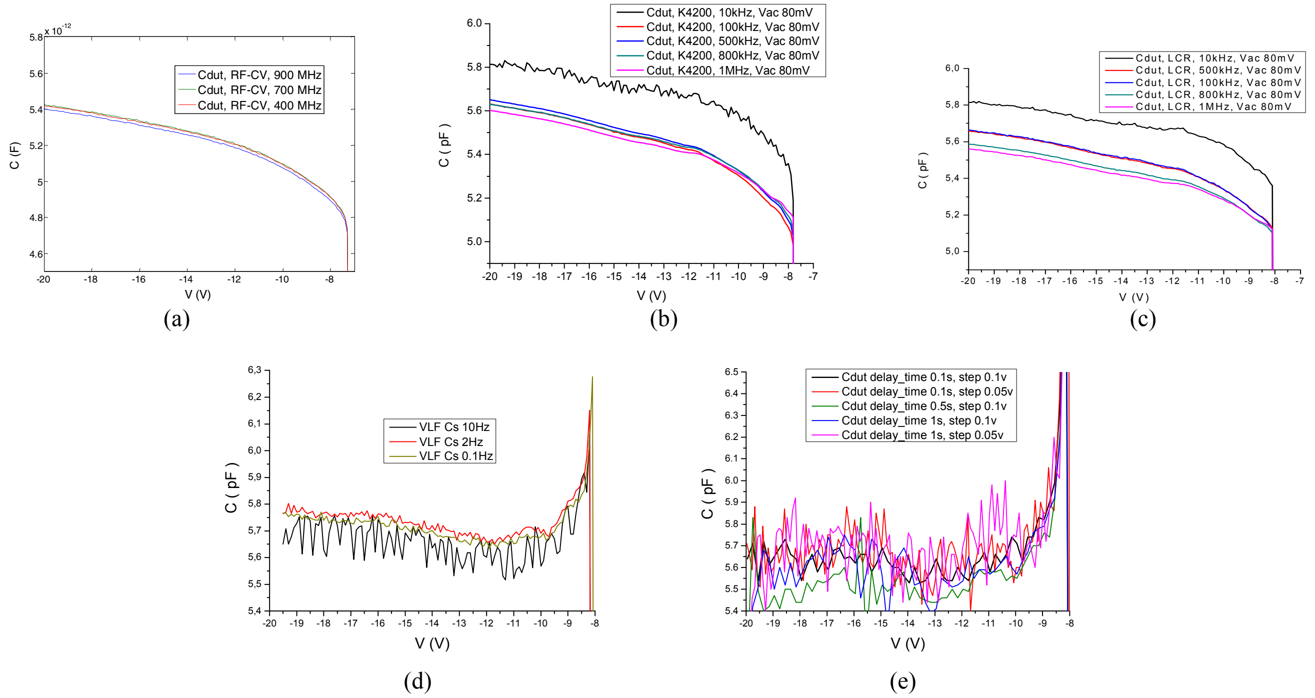

Fig. 7 Comparison of the capacitance of the device in the down-state, (a)RF-CV, (b) K4200, (c) LCR, (d) VLF, (e) QSCV measurements.

C. *Intermediate capacitance state*

We measured an 'intermediate state' between the down-state and the up-state (cf. Fig 6). Fig. 8 zooms in on the intermediate state of the *C-V* curve. The capacitance of this state is 1.5 pF in K4200, LCR and RF-CV measurements and 2 pF according to QSCV and VLF measurements.

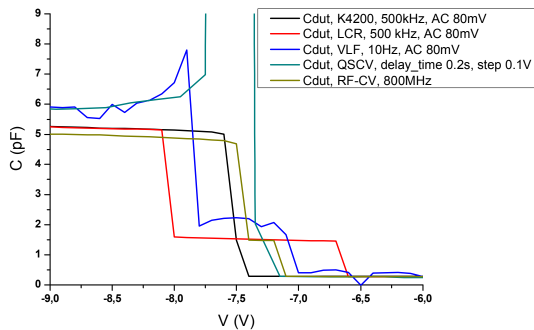

Fig. 8 *C-V* curves measured by five techniques, around the intermediate state observed at pull-out.

To further investigate this intermediate state, the topography of the device was measured by optical means using an MSA-400 Micro-system-analyzer. Fig. 9 (a) shows the topography of the device in the down-state. The red line drawn in the figure runs from the center of the movable top electrode to the fixed end of one anchor. We quantified the height of the device along this line as a function of the applied DC bias. As shown in Fig. 9 (b), the center of the top electrode moves up slightly before the whole electrode comes up, likely corresponding to a lower capacitance than the full down-state. One possible explanation of this behavior is that the top electrode is not flat. The center part is higher than the edge part as a result of the fabrication process. A second factor may be that the electric field at the edge of the electrode is larger than in the center, so the electric force at the edge is larger.

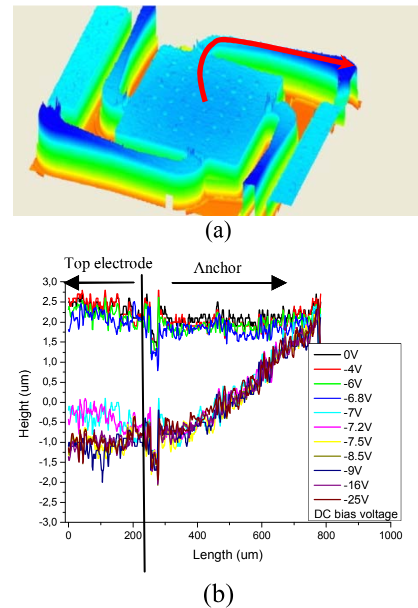

Fig. 9 Dynamic topography of the device, (a) the device in down-state, (b) the height of the surface of the device along the red line in (a) under different DC bias voltages.

According to the measurement results of more than 10 devices, the intermediate capacitance is always there but differs somewhat from device to device. It also changes slightly when we repeat the *V*-sweep measurement. The different capacitance values observed in the intermediate state among different measurements may then be caused by the stiffness of the device.

D. Pull-in voltages

The V_{pi} values measured by the different techniques do not coincide, as shown in Fig. 10. For the RF-CV measurement, V_{AC} was not determined and therefore V_{pi} is indicated with a dashed line. The power of the network analyzer we used for the RF-CV measurement is 0 dB (1 mW). In QSCV, V_{pi} is hard to estimate from the obtained curve; consecutive measurements lead to values randomly differing up to 0.2 V. Hence QSCV values of V_{pi} are not shown in this graph.

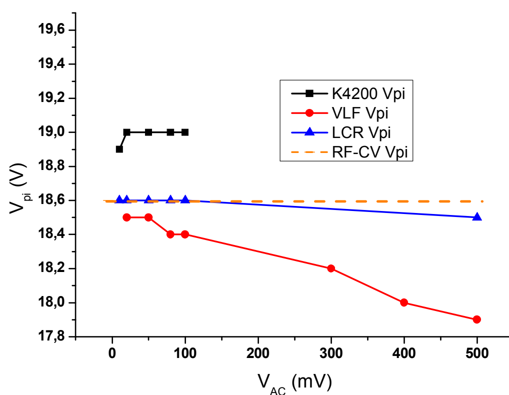

Fig. 10 Pull-in voltage measured by four methods, as a function of the applied ac test signal amplitude.

The observed differences among the pull-in voltages measured by different techniques may be related to device drift. (Note that these are unpackaged devices.) When the test signal has a larger amplitude, the instantaneous electric field may be significantly higher that the DC bias alone, which can lead to earlier pull-in. This is particularly observed with VLF CV measurements (with an almost linear dependence), where the measurement frequency is much lower than the device switching speed.

IV. DISCUSSION

A comparison of the measurement results of these five instruments is made in Table 1 (next page). High-frequency measurements are faster and have better accuracy than QSCV and VLF measurements. The RF-CV and high-frequency measurements, using LCR and K4200 instruments, show similar *C-f* (cf. Fig 5). The *C-V* measurement with the K4200 shows somewhat higher noise in the measurement than the LCR meter (cf. Fig 7b and 7c) but offers multiple functions like DC voltage list sweep, frequency sweep and time sweep.

The VLF and QSCV measurements exhibit higher noise, but do reveal slightly different behavior of the RF MEMS switch which calls for further investigation. Because of the measurement principle, QSCV measurements show unphysical overshoots during pull-in and pull-out. VLF measurement is slower but it can be used for precise measurements on devices with high series resistance (not shown here); it also has multiple functions like high-frequency measurements on the K4200.

V. CONCLUSIONS

The *C-V* curves of RF-MEMS switches measured by five different methods are compared. An equivalent circuit of the parasitics is given. After de-embedding, the device capacitance is almost independent of frequency across 10 orders of magnitude. The device capacitance appears different in the down-state near the pull-out voltage; quasistatic *C-V* and very low frequency measurements yield different results from RF-CV and high-frequency *C-V* measurements. The root cause of this difference is still under study. An intermediate capacitance state was observed at pull-out and associated with the stepwise raising of the moving electrode.

ACKNOWLEDGEMENT

This work has been performed in the EPAMO project, which is funded by public authorities of participant countries as well as by the ENIAC Joint Undertaking.

REFERENCES

[1] J. Bouchaud, "RF MEMS switches, varactors finally penetrate mobile handsets", IHS iSuppli MEMS Market Brief, Vol. 4 issue 12, December 2011.

[2] M. P. J. Tiggelman et al., On the trade-off between quality factor and tuning ratio in high-frequency capacitors, IEEE Trans. El. Dev. 56 (9) 2128 (2009).

[3] P. G. Steeneken et al., *Dynamics and squeeze film damping of a capacitive RF MEMS switch*, J. Micromech. Microeng. 15 (2005) 176–184.

[4] *Performing very low frequency capacitance-voltage measurements on high impedance devices using the model 4200-SCS semiconductor characterization system*, Keithley application note 3140.

[5] J. Schmitz et al., *RF capacitance-voltage characterization of MOSFETs with high leakage dielectrics*, IEEE Electron Device Letters, 24 (1) (2003) 37-39.

[6] Thomas H. Lee, *The design of CMOS radio-frequency integrated circuits*, Cambridge University Press, 2004.

[7] As suggested by R. W. Herfst, private communication, June 2012.

[8] H. M. R. Suy et al., *The static behavior of RF MEMS capacitive switches in contact*, Proceedings of Nanotech MSM, June 2008.

[9] Lifeng Wang et al., *Capacitance characterization of dielectric charging effect in RF MEMS capacitive switches under different humidity environments*, MEMSYS, Jan. 2012.

[10] A. Hariri et al., *Modeling of dry stiction in micro electro-mechanical systems (MEMS)*, J. Micromech. Microeng. 16 (2006) 1195-1206.

[11] A. B. Yu et al., *Effect of surface roughness on electromagnetic characteristics of capacitive switches*, J. Micromech. Microeng. 16 (2006) 2157-2166.

[12] H. M. R. Suy et al., *A Compact Scalable Circuit Model for RF MEMS Switches*, Nanotech MSM, May 2007.

TABLE I. COMPARISON OF THE MEASUREMENTS OF A CAPACITANCE-VOLTAGE SWEEP FROM -20 V TO 20 V (STEP OF 0.1 V) BY FIVE TECHNIQUES

Instrument	QSCV	VLF	K4200	LCR	RF
Typical meas. time	> 1 minute	>> 20 minutes	0,2-2 minutes	1-4 minutes	< 5 seconds
Typical accuracy	≈ 0.1 pF	0.01 pF to 0.1 pF	< 0.001 pF at frequency from 50 kHz to 1 MHz	< 0.001 pF at frequency from 10 kHz to 1 MHz	Calculated from S_{11}
Range of DC voltage sweep	From -20 V to 20 V	From -20 V to 20 V	From -30 V to 30 V	From -40 V to 40 V	From -30 V to 30 V
Range of frequency	N.A.	0.01 Hz to 1 Hz	1 kHz - 10 MHz	20 Hz-1 MHz	80 MHz – 1 GHz
Ease of calibration	Difficult (small compensation noise)	Difficult (small compensation noise)	Easy	Easy	Easy
Artefacts	Yes (near V_{pi} and V_{po})	Yes but small (near V_{pi} and V_{po})	No	No	No
Sweep functions	V-sweep	V-sweep, f-sweep	V-sweep, DC voltage list sweep, f-sweep and time sweep.	V-sweep	V-sweep, f-sweep